NASA/TM—2010-216069 AIAA–2009–4802

Turbofan Volume Dynamics Model for Investigations of Aero-Propulso-Servo-Elastic Effects in a Supersonic Commercial Transport

Joseph W. Connolly and George Kopasakis
Glenn Research Center, Cleveland, Ohio

Kimberly A. Lemon
Wichita State University, Wichita, Kansas

May 2010

NASA STI Program . . . in Profile

Since its founding, NASA has been dedicated to the advancement of aeronautics and space science. The NASA Scientific and Technical Information (STI) program plays a key part in helping NASA maintain this important role.

The NASA STI Program operates under the auspices of the Agency Chief Information Officer. It collects, organizes, provides for archiving, and disseminates NASA's STI. The NASA STI program provides access to the NASA Aeronautics and Space Database and its public interface, the NASA Technical Reports Server, thus providing one of the largest collections of aeronautical and space science STI in the world. Results are published in both non-NASA channels and by NASA in the NASA STI Report Series, which includes the following report types:

- TECHNICAL PUBLICATION. Reports of completed research or a major significant phase of research that present the results of NASA programs and include extensive data or theoretical analysis. Includes compilations of significant scientific and technical data and information deemed to be of continuing reference value. NASA counterpart of peer-reviewed formal professional papers but has less stringent limitations on manuscript length and extent of graphic presentations.

- TECHNICAL MEMORANDUM. Scientific and technical findings that are preliminary or of specialized interest, e.g., quick release reports, working papers, and bibliographies that contain minimal annotation. Does not contain extensive analysis.

- CONTRACTOR REPORT. Scientific and technical findings by NASA-sponsored contractors and grantees.

- CONFERENCE PUBLICATION. Collected papers from scientific and technical conferences, symposia, seminars, or other meetings sponsored or cosponsored by NASA.

- SPECIAL PUBLICATION. Scientific, technical, or historical information from NASA programs, projects, and missions, often concerned with subjects having substantial public interest.

- TECHNICAL TRANSLATION. English-language translations of foreign scientific and technical material pertinent to NASA's mission.

Specialized services also include creating custom thesauri, building customized databases, organizing and publishing research results.

For more information about the NASA STI program, see the following:

- Access the NASA STI program home page at *http://www.sti.nasa.gov*

- E-mail your question via the Internet to *help@sti.nasa.gov*

- Fax your question to the NASA STI Help Desk at 443–757–5803

- Telephone the NASA STI Help Desk at 443–757–5802

- Write to:
  NASA Center for AeroSpace Information (CASI)
  7115 Standard Drive
  Hanover, MD 21076–1320

NASA/TM—2010-216069 AIAA–2009–4802

Turbofan Volume Dynamics Model for Investigations of Aero-Propulso-Servo-Elastic Effects in a Supersonic Commercial Transport

Joseph W. Connolly and George Kopasakis
Glenn Research Center, Cleveland, Ohio

Kimberly A. Lemon
Wichita State University, Wichita, Kansas

Prepared for the
45th Joint Propulsion Conference and Exhibit
cosponsored by the AIAA, ASME, SAE, and ASEE
Denver, Colorado, August 2–5, 2009

National Aeronautics and
Space Administration

Glenn Research Center
Cleveland, Ohio 44135

May 2010

Acknowledgments

The authors would like to acknowledge the Fundamental Aeronautics Program for their support and funding of this work. Additionally, they would like to thank Dan Paxson for sharing his overall aerospace propulsion system modeling experience, thereby furthering their understanding of the subject.

This work was sponsored by the Fundamental Aeronautics Program at the NASA Glenn Research Center.

Level of Review: This material has been technically reviewed by technical management.

Available from

NASA Center for Aerospace Information
7115 Standard Drive
Hanover, MD 21076–1320

National Technical Information Service
5285 Port Royal Road
Springfield, VA 22161

Available electronically at http://gltrs.grc.nasa.gov

Turbofan Volume Dynamics Model for Investigations of Aero-Propulso-Servo-Elastic Effects in a Supersonic Commercial Transport

Joseph W. Connolly and George Kopasakis
National Aeronautics and Space Administration
Glenn Research Center
Cleveland, Ohio 44135

Kimberly A. Lemon
Wichita State University
Wichita, Kansas 67260

Abstract

A turbofan simulation has been developed for use in aero-propulso-servo-elastic coupling studies, on supersonic vehicles. A one-dimensional lumped volume approach is used whereby each component (fan, high-pressure compressor, combustor, etc.) is represented as a single volume using characteristic performance maps and conservation equations for continuity, momentum and energy. The simulation is developed in the MATLAB/SIMULINK (The MathWorks, Inc.) environment in order to facilitate controls development, and ease of integration with a future aero-servo-elastic vehicle model being developed at NASA Langley. The complete simulation demonstrated steady state results that closely match a proposed engine suitable for a supersonic business jet at the cruise condition. Preliminary investigation of the transient simulation revealed expected trends for fuel flow disturbances as well as upstream pressure disturbances. A framework for system identification enables development of linear models for controller design. Utilizing this framework, a transfer function modeling an upstream pressure disturbance's impacts on the engine speed is developed as an illustrative case of the system identification. This work will eventually enable an overall vehicle aero-propulso-servo-elastic model.

Nomenclature

A	Cross sectional area, m^2
APSE	Aero-propulso-servo-elasticity
C_{xy}	Coherence
HSR	High speed research project
HPC	High-pressure compressor
HPT	High-pressure turbine
I	Moment of inertia, $(N*m)/sec^2$
J	Mechanical equivalent of heat, 1 (N*m)/J
K_A, K_B	Unit less combustion coefficient
K_C	Combustion coefficient, $(N^2s^2)/(kg^2m^4K)$
LPC	Low-pressure compressor
LPT	Low-pressure turbine
M	Mach number
N	Rotational speed, rpm
P	Pressure, N/m^2
P_{xx}	Power spectral density about x
P_{xy}	Power spectral density about x and y

P_{yy}	Power spectral density about y
R	Universal gas constant, (N*m)/(kg*K)
T	Temperature, K
T_{xy}	Frequency data for transfer function
Th	Thrust, N
U	Volumetric flow, m^3/s
V	Volume, m^3
$\dot{W}$	Mass flow rate, kg/sec
c_p	Specific heat at constant pressure, J/(kg*K)
f	Frequency, Hz
l	Length, m
s	Laplace variable
u	Velocity, m/s
Δ	Change in variable
ΔP	Combustion pressure loss, Pa
γ	Ratio of specific heats
η	Efficiency
ρ	Density, kg/m^3
τ	Time delay
τ_{flame}	Time delay flame

Subscripts

a	Variable associated with combustion acoustics
ab	Variable associated with afterburner
amb	Ambient condition variable
bleed	Bleed from the high-pressure compressor
bypass	Variable associated with bypass flow
c	Corrected condition
cb	Variable associated with combustor/burner
cool	Coolant flow variable
d	Design condition
exit	Variable associated with exit condition at nozzle
f	Fuel flow into combustor
$\dot{f}$	Fuel flow rate after combustion dynamics
hpc	Variable associated with high-pressure compressor
hpt	Variable associated with high-pressure turbine
inlet	Variable associated with the inlet exit condition
lpc	Variable associated with the fan/low-pressure compressor
lpt	Variable associated with the low pressure turbine
n	Current component volume
ratio	Ratio of variables
ref	Reference variable
sv	Static condition variable associated with stage volume
tc	Total condition variable associated with stage characteristics
tv	Total condition variable associated with stage volume
z	Variable associated with exit nozzle

Introduction

The Aeronautics Research Mission Directorate of the National Aeronautics and Space Administration (NASA) is developing technologies, capabilities, and furthering the aerospace discipline to support all vehicles in the supersonic flight regime, where vehicles are typically longer and slender. For new designs of commercial supersonic vehicles the vehicle shape is expected to be much long, causing any disturbances in the airflow to induce highly complex aeroelastic modes in the vehicle airframe (Ref. 1). While the vehicle is experiencing these nonlinear dynamics, there is a coupling with the vehicle propulsion system. The airframe can introduce disturbances into flow path of the engine, and the thrust will impact loads on the airframe. To ensure success with this project it is critical to understand the Aero-Propulso-Servo-Elastic (APSE) effects. Traditionally, flight control surfaces deal with all vehicle dynamics whereas the engine controls only pertain to the performance of the engine. However, because of the interactions between the airframe and propulsion system, coupling the control of the vehicle dynamics with the control of the propulsion system will ease environmental and performance barriers, such as cruise efficiency, stability, and ride quality (Refs. 2 and 3).

To further the understanding of APSE, NASA Glenn and NASA Langley are building upon past legacies in propulsion and flight vehicle dynamics respectively. Initial efforts are underway to develop the appropriate models for propulsion and flexible airframe dynamics. These models can then be integrated into an overall APSE model. It will be imperative during the integration process that the dominant coupling dynamics between the propulsion system, airframe, and flow fields are understood. This will allow for synergistic control designs that alleviate issues of integrating previously segregated control loops. The focus of the NASA Glenn effort described in this paper is modeling the turbofan engine for the propulsion system.

A component based control volume dynamic turbojet simulation has previously been developed and validated against both experimental and simulated results (Ref. 4). However, a turbofan engine is identified by the High Speed Research (HSR) program as the optimal propulsive system for supersonic flight (Ref. 5). Some of the benefits of a turbofan engine compared to a turbojet engine include increased propulsive efficiency and decreased noise. Using the turbojet simulation as a starting point, a turbofan simulation has been developed. This turbofan simulation comprises a component of the propulsion dynamics making up the overall integrated performance model.

The modeling effort is presently focused on the cruise condition. To determine the appropriate model for this task it is important to consider the ability to capture the relevant dynamics, ease of model integration into an overall APSE model, and suitability for the development of controls. While many previous models are capable of capturing dynamic behavior of a turbofan engine, few exist that allow for easy integration with preexisting MATLAB simulations (Refs. 6 to 8). Therefore, the platform chosen for development is MATLAB/SIMULINK, because it fulfills all of the requirements listed above. Its compatibility with previous aero-servo-elastic models developed at NASA Langley and its built-in tools will allow for easier controls development. This paper provides a broad overview of supersonic propulsion system modeling followed by a detailed discussion on engine modeling development, simulation performance results, a system identification approach leading to controls development, and how the engine model fits into the larger APSE model.

Engine Modeling

The overall propulsion system for the vehicle is comprised of a supersonic mixed compression inlet and engine. The engine is connected just downstream of the inlet flow path. Previous research from the HSR program looked into several engine designs and found that low bypass turbofan engines are desirable (Ref. 5). However, due to a lack of detailed non-proprietary information for turbofan engines the modeling effort done previously under the APSE task was for a turbojet engine, the GE J-85 (Ref. 4). The J-85 has undergone extensive testing at NASA Glenn, and has been used in supersonic vehicles. Having access to data that includes many of the required performance parameters allowed for easier model

development and verification. The work presented here is an extension of the previous work. The engine modeled represents a notional, medium size bypass turbofan engine that would be suitable for a business class supersonic jet.

A generic turbofan engine schematic is illustrated in Figure 1. This particular design would be too small for the larger commercial passenger jet that is being investigated for the NASA supersonics project. However, this engine is useful for developing the appropriate modeling capability for when the project begins to narrow its focus to a particular engine design.

In many scenarios a low fidelity engine model that captures only the slow dynamics due to typical flow disturbances and the fuel control/actuation system is adequate. These dynamics lend themselves to a smaller control bandwidth and thus allow for the low fidelity models to be adequate for control design (Refs. 10 and 11). As such, the engine dynamics are driven primarily by the shaft moments of inertia. However in future supersonic vehicles, higher frequency (approximately 50 Hz) upstream flow disturbances induced by the vibrations in the vehicle are expected. Also new engines are expected to operate closer to the limits of their capability, (e.g., with reduced surge margins). More accurate models are expected to be required. For these reasons a nonlinear one-dimensional lumped volume approach is used in the SIMULINK environment, as opposed to a model with dynamics only associated with the energy balance of the rotating shafts.

While a particular turbofan engine design is discussed in this paper, the model is developed with the goal of easy adjustments allowing for simulating any particular turbofan engine. The modeling effort is based on previous work done by Seldner utilizing an analog computer (Ref. 12). The SIMULINK model developed for this study uses data provided for steady state flow parameters from a paper-designed engine output from the Numerical Propulsion System Simulation code developed in house at NASA Glenn for the purposes of steady state verification (Ref. 13). Since many design decisions are still to be determined in this project, the primary focus is on developing a feasible approach to solve the desired problem and on capturing the expected trends in the model. Later, when project decisions are made for a particular engine, more focus can be placed on the steady state values and on ensuring that more than just the expected transient trends are modeled to the appropriate fidelity.

Currently the model uses a single lumped volume for each of the major components consisting of the low-pressure compressor (LPC) or commonly referred to as the fan, the high-pressure compressor (HPC), the combustor, the high-pressure turbine (HPT), the low-pressure turbine (LPT), the mixer/afterburner, the low-pressure shaft, the high-pressure shaft, and the nozzle. This currently meets the required dynamic bandwidth. However, if added resolution is deemed necessary the model is structured in such a way that it could be used as a stepping-stone to stage-by-stage lumped volume of the compressor and turbine components. A schematic of a generic turbofan engine model can be seen in Figure 2, comprised of the major components discussed above. Given this approach, the required thrust variation needed to couple the propulsion system to the aero-servo-elastic model is obtained. Investigation of the atmospheric and the induced aero-servo-elastic disturbances that feedback into the propulsion system model are still in progress. Ultimately, these will be used to determine realistic disturbance attenuation methods when a fully integrated APSE model is developed. Generic disturbances in the output of the inlet into the flow field of the engine face in terms of pressure are simulated as well as fuel flow disturbances. The use of measured flow field disturbances is planned for future studies.

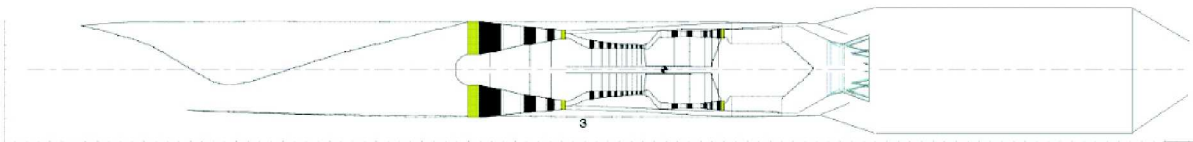

Figure 1.—Generic turbofan engine model resembling current design (Ref. 9).

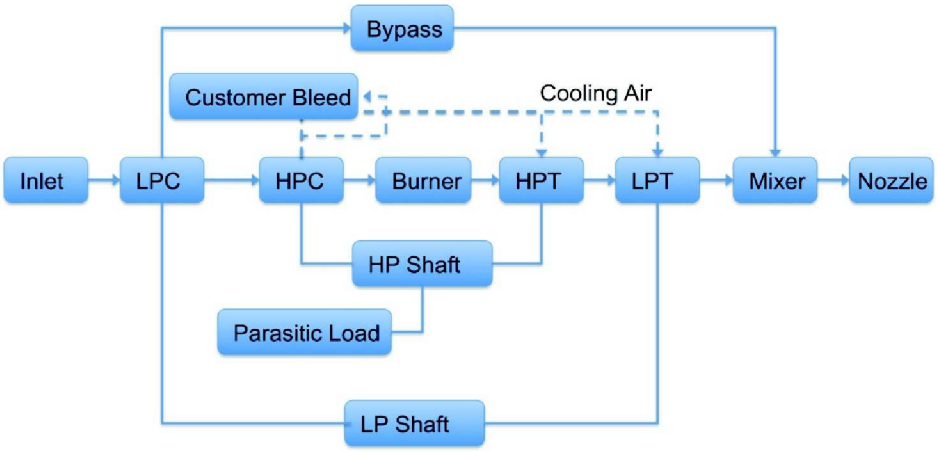

Figure 2.—Turbofan engine schematic (Ref. 9).

Overall Engine Modeling Approach

The modeling approach is derived from work by Seldner and refined in Kopasakis and Stuber for a turbojet engine (Refs. 4, 12, and 14). The equations are given here for completeness and clarity when ultimately integrating into the overall propulsion model. In addition, the equations here are defined for a turbofan with each component being a lumped volume instead of the stage-by-stage development of the equations, as used in previously mentioned work. Each of the fluid flow components are modeled using a set of derived conservation equations modified from the standard form and written in total condition form, where Equations (1) to (3) are the continuity, momentum, and energy equations respectively.

$$\frac{d}{dt}\left(\rho_{sv}\right) = -\frac{1}{v}\Delta\dot{W} \tag{1}$$

$$\frac{d}{dt}\left(\dot{W}\right) = -\frac{A}{l}\Delta P_{tv} \tag{2}$$

$$\frac{d}{dt}\left(\rho_{sv}T_{tv}\right) = -\frac{\gamma}{V}\Delta\left(T_{tv}\dot{W}\right) \tag{3}$$

The total flow property conditions are used for Equations (1) to (3) to allow for easier use with the required performance maps of each component. A performance map allows for the general modeling approach to simulate engines of a particular design, by providing the appropriate pressure ratios and efficiencies. In order to obtain the maps used in this study, a generic map is created using an internal map generation routine, which closely approximates the operating condition of the turbofan engine. This is a source of some disagreement in the dynamic model and steady state data, as the actual map of the engine is not used. This will have a greater impact for dynamic results as the shape of the speed lines will vary, but if the operating condition is not matched exactly errors in steady state can be encountered as well. To avoid the errors and ensure stability each component of the turbofan engine is first modeled individually. Once the individual component models are able to match the expected performance the entire turbofan engine is integrated, allowing for simple resolution of errors that could otherwise be compounded.

Low Pressure Compressor

The low-pressure compressor provides a large mass flow rate at the exit to increase the thrust, while keeping the noise generated relatively lower than comparable turbojet engines. The three state variables chosen for the model of each component are the total pressure, total temperature, and mass flow rate.

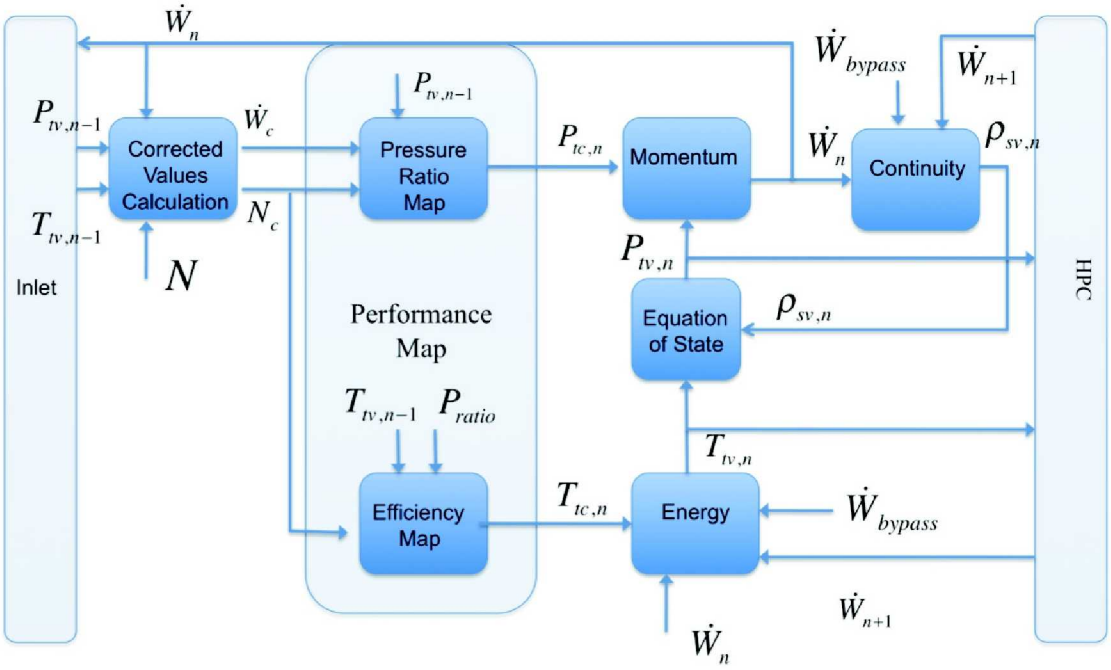

Figure 3.—Low-pressure compressor modeling schematic.

Since this is a subsonic system, information from two of the states must travel downstream, while the other travels upstream. Here the mass flow rate travels upstream and the temperature and pressure travel downstream. A general schematic of the overall modeling approach for the low-pressure compressor can be seen in Figure 3. This schematic is analogous to the other major components, with the exception of various performance maps, which may or may not be required to meet characteristic flow parameters. The variables are left generic and the subscript '*n*' is associated with the current volume.

The incoming flow conditions to the LPC are from the supersonic mixed compression inlet. These conditions are used with performance maps to generate characteristic values for this particular engine design. The LPC performance map is actually two table lookups in the model to obtain a given pressure ratio and efficiency, which are then used to get the characteristic pressure and temperature. The table lookups are based on the corrected mass flow and corrected engine speed line defined respectively in Equations (4) to (5) as

$$\dot{W}_c = \frac{\dot{W}\sqrt{T_{tv}/T_{\text{ref}}}}{P_{tv}/P_{\text{ref}}} \tag{4}$$

$$N_c = \frac{N}{N_d}\sqrt{\frac{T_{\text{ref}}}{T_{tv}}} \tag{5}$$

The characteristic performance properties of the compressor are obtained through the performance map and the following two expressions (Eqs. (6) to (7))

$$P_{lpc,tc} = P_{lpc,\text{ratio}} P_{\text{inlet},tv} \tag{6}$$

$$T_{tc} = T_{\text{inlet},tv}\left(1+\frac{P^{\frac{\gamma_{lpc}-1}{\gamma_{lpc}}}_{lpc\,\text{ratio}}-1}{\eta_{lpc}}\right) \tag{7}$$

Once the characteristic properties of the temperature and pressure are obtained from the map, they are used in the conservation equations for the low-pressure compressor, (Eqs. (8) to (13))

$$\frac{d}{dt}\rho_{lpc,sv} = \frac{1}{V_{lpc}}\left(\dot{W}_{lpc} - \dot{W}_{hpc} - W_{\text{bypass}}\right) \tag{8}$$

$$\frac{d}{dt}\dot{W}_{lpc} = \frac{A_{lpc}}{l_{lpc}}\left(P_{lpc,tc} - P_{lpc,tv}\right)\left\{1+\frac{\gamma_{lpc}-1}{2}M^2\right\}^{\frac{-\gamma_{lpc}}{\gamma_{lpc}-1}} \tag{9}$$

$$\frac{d}{dt}\left(T_{lpc,sv}\rho_{lpc,sv}\right) = \frac{\gamma_{lpc}}{V_{lpc}}\left(T_{lpc,tc}\dot{W}_{lpc} - T_{lpc,tv}\dot{W}_{hpc} - T_{lpc,tv}\dot{W}_{bypass}\right) \tag{10}$$

To interconnect the equations as illustrated in Figure 3, the following state equation is used, Equation (11):

$$P_{tv} = \rho_{sv}RT_{tv}\left(1+\frac{\gamma-1}{2}M^2\right)^{\frac{1}{\gamma-1}} \tag{11}$$

In Equation (11), the expressions use Mach number to correct for the static to total conditions. This will not have much impact on steady state results, but the error associated with the Mach number correction term can be up to 15 percent for the dynamic results depending on flow speed (Ref. 12). The Mach number is calculated using the simple expression in Equation (12)

$$M = \frac{\dot{W}}{\rho_{sv}A\sqrt{\gamma RT_{sv}}} \tag{12}$$

Where the static temperature is obtained by:

$$T_{sv} = T_{tv} - \frac{\dot{W}^2}{2\rho^2A^2c_p} \tag{13}$$

High Pressure Compressor

The high-pressure compressor is modeled using a single lumped volume and a characteristic performance map that is essentially the same method as the low-pressure compressor. One difference is that the low-pressure compressor has a bypass separating the inlet flow into one that travels down the core of the engine and one that moves around the engine. In addition the high-pressure compressor has a bleed that is used to provide cooling air to the high and low-pressure turbine and other systems outside of the engine. The equation for the bleed is shown in Equation (14)

$$\dot{W}_{\text{bleed}} = K_{\text{bleed}} A_{\text{bleed}} \frac{P_{hpc,tv}}{\sqrt{T_{hpc,tv}}} \tag{14}$$

Combustor

Little information was readily available about the actual combustion performance parameters of the combustor. Without too much loss of accuracy a dynamic modeling approach for a lean combustor is used here, which will be more representative of the future combustors to be used for supersonic flight (Ref. 15). The model of the combustor has the usual lumped volume of the flow dynamics and in addition, a simple representation of combustion dynamics are modeled. The key to the modeling approach is to obtain the correct pressure drop across the combustor that is caused by the fluid friction and heat addition. The overall approach can be seen in Figure 4.

The modeling approach for the simple representation of the combustion dynamics uses a transfer function to model the delay that is caused by the actual combustion of the fuel flowing into the combustor. The total delay of the combustion process is a sum of the transport and mixing, the flame dynamics, and the acoustic delays as shown in Equation (15):

$$\tau_{cb} = \tau_t + \tau_{\text{flame}} + \tau_a \approx \frac{V_{cb}}{U_{cb}} \tag{15}$$

For the lean combustor, the total delay is typically approximately 5 msec, where the vast majority of the delay comes from the mixing process(Ref. 15). The actual delays of the individual components that make up the total combustion delay can at times be hard to obtain, and thus a close approximation of the delay can be obtained by dividing the volume with the volumetric flow as seen in Equation (15). The transfer function for the combustion dynamics can then be represented by Equation (16):

$$\frac{\dot{W}_f}{\dot{W}_f} = \frac{e^{-\tau_t s}}{(\tau_{\text{flame}} s + 1)(\tau_a s + 1)} \tag{16}$$

Two maps are used to obtain values required for the conservation equations to appropriately account for heat addition and efficiency. The efficiency here is defined as the amount of heat used to increase the overall temperature in the combustor in relation to the total amount of heat generated from the combustion process and is illustrated in Figure 5 (Ref.12).

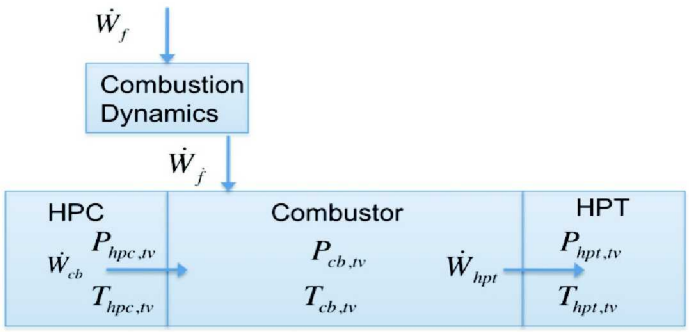

Figure 4.—Combustor lumped volume model schematic.

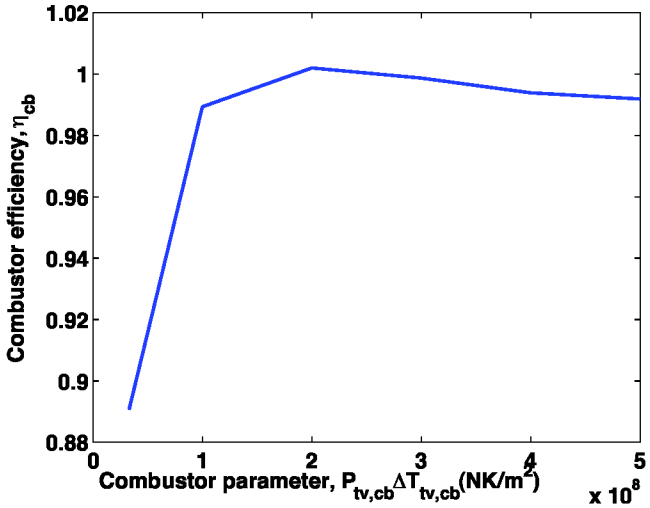

Figure 5.—Combustor efficiency performance map.

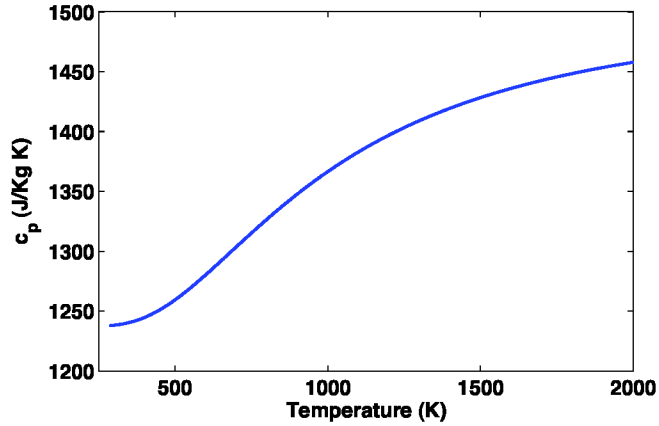

Figure 6.—Specific heat at constant pressure versus temperature.

During the combustion process, fuel is being mixed with the incoming airflow, which alters the chemical makeup of the flow. This, in addition to the significant amount of heat addition, can have a large impact on the assumed specific heat of the flow. The variation of the specific heat at constant pressure can be obtained from the NACA Report 1135, which is plotted in Figure 6 (Ref. 16). The specific heat at constant pressure data is then used as a look up table in the model.

The next key factor that needs to be obtained for the combustor model is the loss of pressure. This can be defined as losses due to friction, $K_A = 0.771$, and heat addition, $K_B = 0.085$. The loss coefficients are obtained through experimental testing, non-combustion flow testing and combustion flow testing respectively. Given the experimentally obtained values, the pressure loss can be expressed by Equation (17):

$$\Delta P_{cb,tv} = \frac{K_C \dot{W}_{cb}^2}{P_{hpc,tv}} \left(0.771 T_{hpc,tv} - 0.085 T_{cb,tv}\right) \tag{17}$$

The value of K_C is obtained using a range of steady state values and assuming a pressure loss between 1 to 5 percent, to create a table lookup over the given range of values. The conservation equations can be solved using the above data for a specific combustor design, and are in the Appendix.

The enthalpy in Equation (34), shown in the appendix, is a constant for JP-4 fuel at 1000 K (Ref. 17). The equation of state is then used to tie the conservation equations together as is done in the compressor model. Here a correction factor using the Mach number is not used, in part, because the flow in the combustor is generally moving relatively slowly. The one change to the state equation is that the gas constant must change to take into account the change in the fluid properties due to the addition and reaction of fuel.

High Pressure Turbine

The turbine model is effectively the same as the compressor with the following exceptions: different performance maps are used and instead of compressing the fluid the turbine rapidly expands the fluid. Corrected speed and mass flow rate are again used in conjunction with a performance map to obtain the characteristic pressure and temperature of the turbine. The same modeling approach from Figure 3 is used.

In developing the turbine model, the same basic form of the corrected compressor conditions can be used. The significant difference here is that the pressure ratio obtained from the performance map is the inverse of that obtained from the compressor. The inversion of the pressure ratio then results in the alteration of the expression for the characteristic pressure and temperature of the turbine in Equations (18) to (19).

$$P_{hpt,tc} = \frac{P_{cb,tv}}{P_{hpt,\text{ratio}}} \tag{18}$$

$$T_{hpt,tc} = T_{cb,tv}\left(1 - \eta_{hpt}\left(1 - P_{hpt,\text{ratio}}^{\frac{-\gamma_{hpt}-1}{\gamma_{hpt}}}\right)\right) \tag{19}$$

The characteristic values are then used in the conservation equations for the high-pressure turbine found in the appendix. The Mach number correction is again used in the conservation equations since the speed of the flow is higher and can cause an even greater error in the dynamic response of the turbine than in the compressor. The equation of state is used to link the conservation equations together, with the modification that the gas constant must account for the fuel added to the flow during combustion and increased airflow from the compressor for cooling.

Low Pressure Turbine

The low-pressure turbine is modeled in exactly the same manner as the high-pressure turbine. The differences are that different performance maps are used and the coolant required to operate at a reasonable temperature is less than that of the HPT. The conservation equations are presented in the Appendix for completeness.

Mixer/Afterburner

The mixer and afterburner are modeled together, which is a slight deviation from the turbofan engine model that is to be matched in this work. The deviation is that the steady state data is obtained from a turbofan engine model that does not have an afterburner. However, an engine for the larger supersonic commercial vehicle may require an afterburner. To allow for more modeling flexibility the afterburner's combustor is coded to allow for combustion. However, it is assumed to be a non-combusting design, i.e. no fuel added. This allows for the appropriate equations for an afterburner with the option of using it as a simple mixing cold pipe. The Concorde is an example of supersonic flight where an afterburner is used,

but only ignited during takeoff and powering though the transonic regime (Ref. 2). In the study here, the interest is in the cruise condition. Thus a non-combusting afterburner meets the requirements. The mixer/afterburner essentially acts as a volume that is capable of attenuating disturbances and mixes the bypass flow with the core flow for exhaust through a common nozzle. The conservation equations are expressed in the Appendix.

Exit Nozzle

The nozzle of a turbofan expels both the core flow and the bypass flow into the atmosphere. The following series of equations can be used to obtain the exit mass flow rate, Equation (23), which is then simply multiplied by the exit velocity to obtain the gross thrust of the engine, Equation (24). The first step is to obtain an estimate of the Mach number, Equation (20). Then the static temperature can be obtained, Equation (21), which allows for the calculation of the local speed of sound, Equation (22). The nozzle efficiency is a ratio of the actual change in kinetic energy to the ideal change, and is assumed constant at $\eta_z = 0.98$

$$M^2 = \frac{2}{\gamma_{ab} - 1}\left[\frac{\eta_z\left(1 - \frac{P_{amb}}{P_{ab}}^{\frac{-\gamma_{ab}-1}{\gamma_{ab}}}\right)}{1 - \eta_z\left(1 - \frac{P_{amb}}{P_{ab}}^{\frac{-\gamma_{ab}-1}{\gamma_{ab}}}\right)}\right] \tag{20}$$

$$T_{sv} = \frac{T_{tv}}{1 + \frac{\gamma_{ab-1}}{2} M^2} \tag{21}$$

$$a = \sqrt{\gamma_{ab} T_{sv} R} \tag{22}$$

$$\dot{W}_z = \rho M a A_{\text{exit}} \tag{23}$$

$$Th = \dot{W} u_{\text{exit}} \tag{24}$$

Low and High Pressure Shafts

For the engine to reach a steady state condition there needs to be an energy balance for each of the rotating spools. The low-pressure spool connects the low-pressure compressor that does work and low-pressure turbine that extracts work. If there is an imbalance in the torque provided by each component the spool accelerates, governed by Equation (25).

$$\frac{dN_{lp}}{dt} = \left(\frac{30}{\pi}\right)^2 \left(\frac{J}{N_{lp} I_{lp}}\right)\left[\left(h_{hpt}\dot{W}_{lpt} + h_{hpc}\dot{W}_{lpt,\text{cool}} - h_{lpt}\dot{W}_{ab}\right) - \left(h_{lpc}\dot{W}_{hpc} + h_{lpc}\dot{W}_{\text{bypass}} - h_{\text{inlet}}\dot{W}_{lpc}\right)\right] \tag{25}$$

The high-pressure spool interconnects the high-pressure compressor and the high-pressure turbine, and is governed by Equation (26).

$$\frac{dN_{hp}}{dt} = \left(\frac{30}{\pi}\right)^2 \left(\frac{J}{N_{hp} I_{hp}}\right) \left[\left(h_{cb}\dot{W}_{hpt} + h_{hpc}\dot{W}_{hpt,\text{cool}} - h_{hpt}\dot{W}_{lpt}\right) - \left(h_{hpc}\dot{W}_{cb} + h_{hpc}\dot{W}_{\text{bleed}} - h_{lpt}\dot{W}_{hpc}\right)\right] \quad (26)$$

Engine Simulation Results

The results shown here highlight the ability of the turbofan engine model to meet steady state results and provide reasonable transient responses to disturbances of the incoming pressure, fuel flow, and their impacts on thrust for a supersonic propulsion system. The simulation is run for a flight cruise condition for the commercial supersonic vehicle at 60,000 ft and at a Mach number of 2.35. The engine model starts at the exit of the inlet where the pressure is 88211.52 Pa and the temperature is 454.87 K, using the described cruise condition. A SIMULINK built in integration scheme is used that implements a variable time step explicit Runge-Kutta method (Ref. 18). The first part of the presented results will cover matching of the dynamic model steady state performance to that of the static Numeric Propulsion System Simulation model. Then the response to fuel flow disturbances is investigated as this will be important in the future work of developing control algorithms. Finally, the response to incoming pressure disturbances, that are to simulate disturbances in the upstream flow field, are presented.

Overall Engine Performance Steady State

The steady state results are simulated for the cruise condition operating at 100 percent power. Table 1 shows the summary of output from both models for the high-pressure components. The model currently does not have a throttle setting implemented, so the high-pressure shaft corrected speed is used in Table 1. On the left hand side of the table each model is listed: static for the one we are trying to match, and dynamic for the SIMULINK developed dynamic model. The last row provides a percent error between the two models. The values for each table are given in SI units of Pascal for pressure, Kelvin for temperature, and Kg/s for mass flow. The high-pressure components have a very good matching, with the largest error being in the compressor output temperature, 4.38 percent.

TABLE 1.—STEADY STATE PERFORMANCE FOR HIGH-PRESSURE COMPONENTS

Model	Corr. speed %	High pressure compressor			Combustor			High pressure turbine		
		P	T	$\dot{W}$	P	T	$\dot{W}$	P	T	$\dot{W}$
Static	100	1269021	999.2	39.4	1211705	1922	30.7	371613	1420	31.6
Dynamic	**99.9**	**1277813**	**1043**	**39.3**	**1220708**	**1969**	**30.6**	**370677**	**1462**	**31.5**
Error %	0.1	0.69	4.38	0.25	0.74	2.45	0.33	0.25	2.96	0.32

Table 2 shows the summary of the output from both models for the low-pressure components, at the cruise condition, operating at 100 percent corrected speed for low-pressure shaft. The low-pressure components also match very well for the steady state results, where the largest error is in the LPT temperature. One common theme for both tables is that the greatest error seems to come from the temperature. The error for both tables is due in part to not exactly matching the operating point. The very slight error in the speed can causes errors due to incorrect maps being used. Another source of error is the use of a bleed calculation based on HPC flow parameters, Equation (14). The cooling air for the HPT and LPT is then a percentage of that bleed. When developing the individual component model, a static bleed was used, which provided good matching. However, the calculated bleed is used instead of a static bleed, because during transient events it was found that the simulation was more stable with a varying bleed.

TABLE 2.—STEADY STATE PERFORMANCE FOR LOW-PRESSURE COMPONENTS

Model	Corr. Speed %	Low Pressure Compressor			Low Pressure Turbine			Mixer/Afterburner		
		P	T	$\dot{W}$	P	T	$\dot{W}$	P	T	$\dot{W}$
Static	100	194707	579	80.8	172231	1186	40.1	173865	892	40.1
Dynamic	**99.94**	**193630**	**581**	**80.7**	**172480**	**1228**	**40.0**	**172480**	**896**	**39.3**
Error %	0.06	0.55	0.35	0.12	0.14	3.54	0.23	0.80	0.45	1.99

Fuel Flow Disturbance

The fuel flow disturbance is introduced by stepping the fuel flow up and down by 1 percent. This has a direct impact on the temperature in the fluid flow of the turbofan core. To illustrate the transient response, the low-pressure turbine output temperature is plotted in Figure 7.

The input disturbance can be seen on the bottom of Figure 7 and the response is on the top. One key thing that is illustrated in this figure is that the up and down response is comparable in magnitude and shape. This is important because it will allow for easier linear model development. A closer look at a particular step in the fuel flow can be seen in Figure 8. The response has a slight delay as is expected with the combustion dynamics, a small overshoot, and then quickly settles out in approximately 0.1 sec. Notionally similar results to fuel flow disturbances can be seen in Daniele and Khalid (Refs. 6 and 19).

The main purpose of this work is to understand how disturbances impact the thrust. Therefore we want to develop a controller that can mitigate thrust perturbations. However, thrust is not typically a measurement that is available to the control algorithm. To control the thrust a relation is usually developed between the speed of the turbofan and the output thrust. In Figure 9, the low-pressure shaft speed and output thrust can be seen as a result of a disturbance in the fuel flow. The response shows a relatively smooth exponential response to the steady state value after the step, and settles again in less than half a second. This provides the shaft speed response shape, shown in other simulations, but this is only a preliminary comparison and further investigation is needed (Refs. 6 and 20).

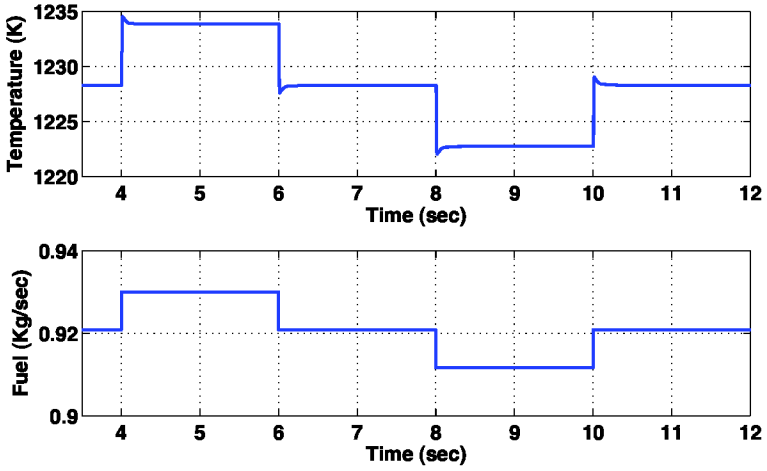

Figure 7.—Fuel flow step disturbance and LPT temperature response.

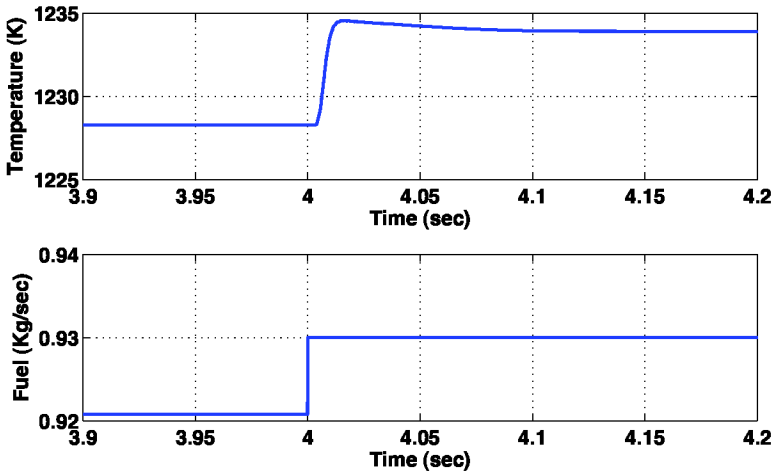

Figure 8.—Fuel flow step disturbance and LPT close up response.

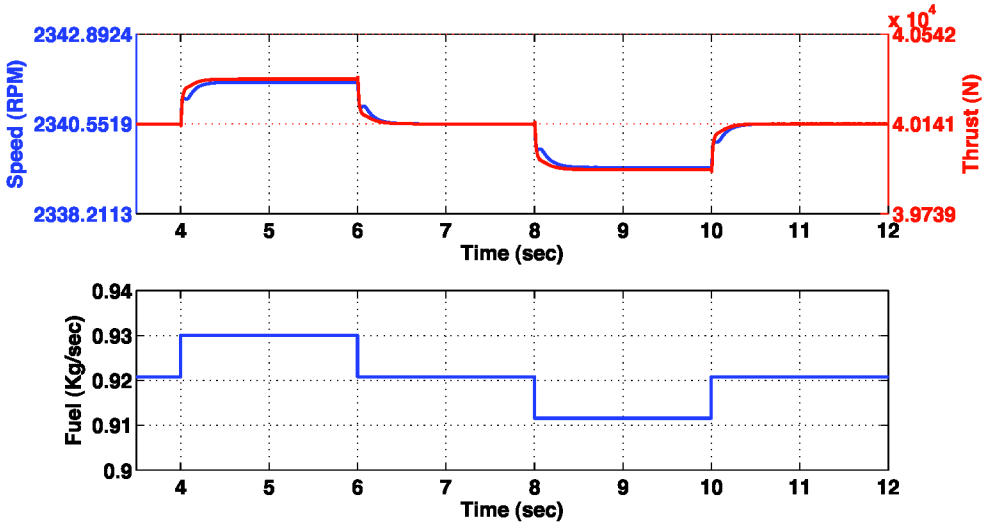

Figure 9.—Fuel flow step disturbance with low-pressure spool speed and thrust response.

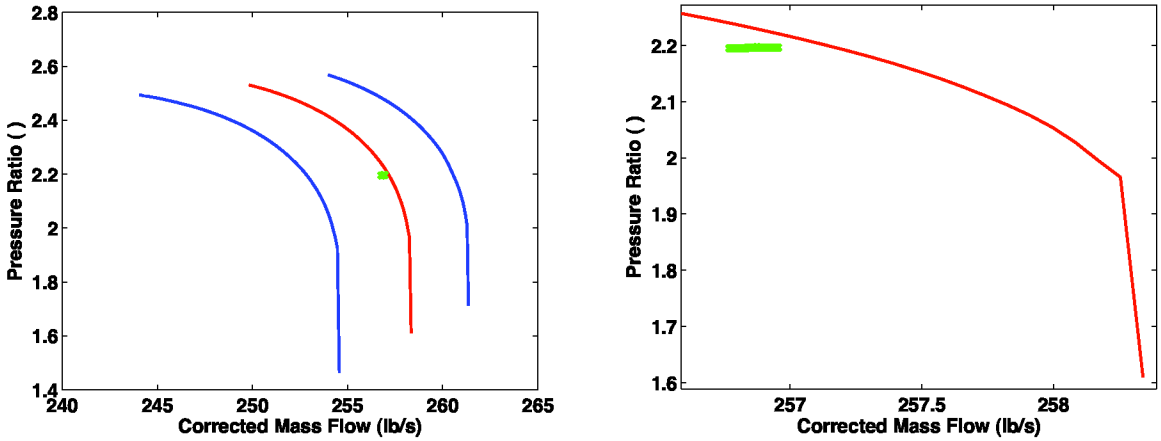

Figure 10.—Low-pressure compressor performance map about the 100 percent speed line and close up of operating point movement due to fuel disturbance.

Another area that is important to investigate is to ensure that movement and operation on the performance map is as expected. In Figure 10, a plot of the low-pressure compressor performance map is illustrated with the engine operating points for the first 5.5 sec of the simulation, covering the step up in fuel flow. The red line is the 100 percent speed line, and the green is the operating location. The steady state point is closest to the 100 percent speed line and then moves away toward the stall during the disturbance. It is expected however that the line should track the shape of the speed line more accurately, and further investigation is required.

Pressure Disturbance

The pressure disturbance is used to crudely mimic the effects of flight through atmospheric disturbances. The disturbance is one percent of the magnitude of the inlet exit total pressure, and again plotted on the bottom of the output response in the following figures. Several of the output parameters, LPC exit pressure and thrust, are plotted to illustrate the response. In Figure 11 it can be seen that the fan pressure response is symmetric as is the case for the fuel flow disturbance. The one significant change in the response however is the sharp overshoot before the transient eventually settles out, which takes approximately 0.11 sec. The larger overshoot should not cause any problem, as it should be dampened out once a controller is implemented. Overshoot in compressor exit pressure due to an upstream pressure disturbances can also be seen in work by Chun (Ref. 15).

The thrust response is illustrated in Figure 12 to demonstrate how the aircraft disturbance signal impacts the propulsion system for the future work of the overall integrated model and control algorithms.

System Identification

The first step in nearly any control design is to understand the required control objective. For this project the goal is to control the thrust of the engine using the fuel flow rate into the combustor. Added fuel increases the energy of the flow and thus increases the thrust. The second step is to obtain a linear model of the relevant dynamics of the non-linear plant model. To obtain the linear models, some of the tools provided by MATLAB's system identification and signal processing toolbox are used. Sinusoidal sweeps are used to perturb the nonlinear models allowing for the creation of transfer functions over the relevant frequency range.

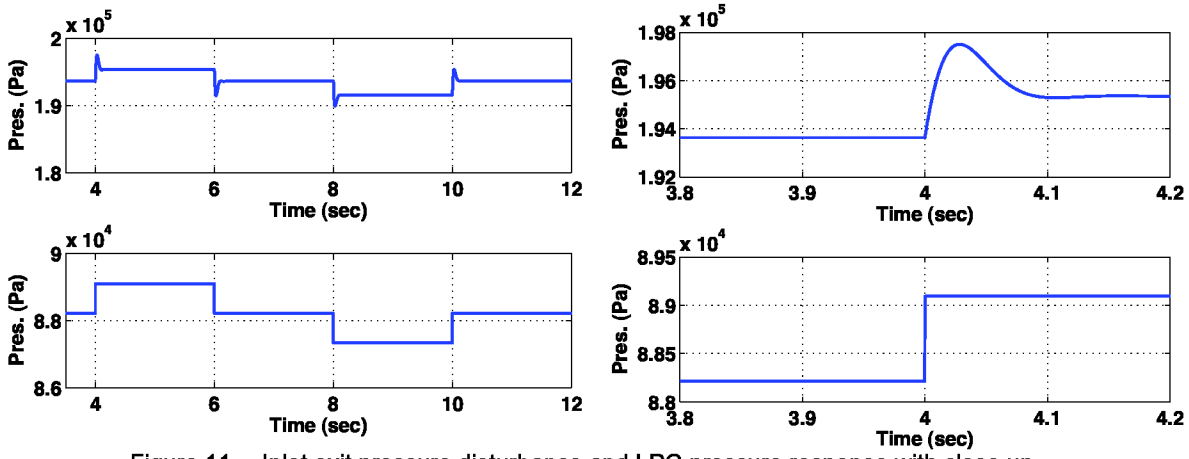

Figure 11.—Inlet exit pressure disturbance and LPC pressure response with close up.

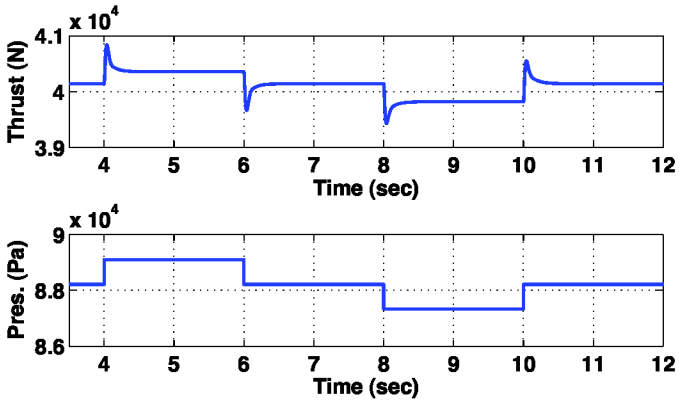

Figure 12.—Inlet exit pressure disturbance and thrust response.

To start the process of creating linear models Welch's average modified periodogram method is utilized, where an estimate of the power spectral density is obtained (Ref. 22). The basic idea is simple in that one takes an input vector of data, x, and an output vector of data, y, and uses Welch's method to generate data for a transfer function. This is obtained by the cross power spectral density of x and y divided by the power spectral density of x in Equation (27):

$$T_{xy}(f) = \frac{P_{xy}(f)}{P_{xx}(f)} \tag{27}$$

This then provides the data to generate a transfer function over a given frequency range, f, where a transfer function is defined here as the actual poles and zeros needed to match the frequency response due to the perturbation input signal. To gage how well this method estimates the actual dynamics, the coherence between the signals is computed, which can give valuable insight. Again using Welch's method, the coherence looks at the magnitude squared of the cross spectral density of the input and output signal, divided by the power spectral density of each signal in Equation (28):

$$C_{xy}(f) = \frac{\left|P_{xy}(f)\right|^2}{P_{xx}(f)P_{yy}(f)} \tag{28}$$

This provides a vector of the coherence ranging from one to zero over a desired frequency range. A value of one signifies that the input vector corresponds highly with the output vector. This information is important here, in attempting to model a highly nonlinear system using a linear approach. If the disturbance signal we are applying to the model has too large a magnitude, the corresponding output will have a high level of nonlinearity, and the coherence of our estimate will be close to zero.

The expected dynamics that are of interest to this study are the flow perturbations induced by the vibrating airframe. The frequency range for these dynamics is assumed to be approximately 50 Hz (Ref. 23). The sinusoidal frequency sweep used to generate the linear models is from a minimum frequency of 0.1 Hz and a maximum of 1000 Hz. To gain a better understanding of the actual system identification approach, an inlet exit pressure disturbance will be used as an illustration. Figure 13 shows the sinusoidal inlet exit pressure disturbance in the bottom subplot. The top subplot illustrates on the right hand y-axis, the change in the disturbance frequency over time corresponding to the green line. The left hand y-axis illustrates the response of the speed of the Low-pressure spool. The plot here is limited to that part of the sweep below 150 Hz to allow for the lower frequency response to be more easily seen, as it is more pertinent to the expected disturbances.

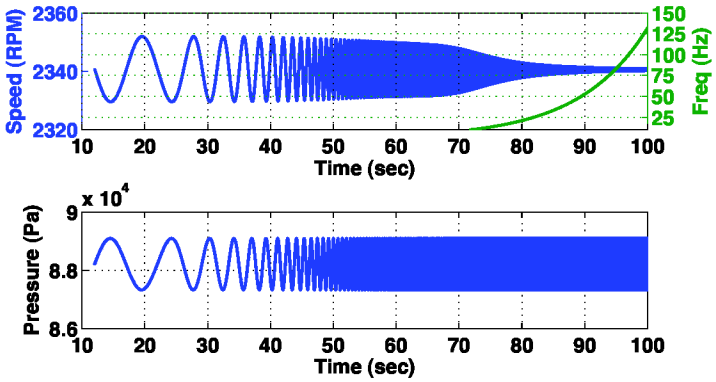

Figure 13.—Inlet exit pressure disturbance and low-pressure shaft speed response.

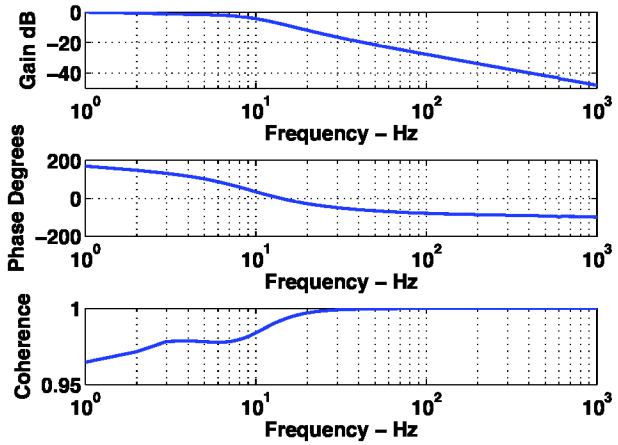

Figure 14.—Bode plot of transfer function data of an inlet exit pressure disturbance to the low-pressure spool speed response.

Figure 13 provides a plot of the input and output vectors used by Welch's method to generate the data for the transfer function estimate of inlet exit pressure disturbance to low-pressure shaft speed. The output from this method is then used to generate a Bode plot to ensure that the modeled dynamics are reasonable.

Depicted in Figure 14 is a Bode plot of magnitude and phase, along with the coherence to ensure the data is a good fit. The coherence shows that there is a strong correspondence between the input and the output vectors. This implies that the estimate of the transfer function is reasonable, with only a slightly lower coherence in the 10 Hz and below range. The transfer function estimate indicates that the linear model should have an adequate ability to model disturbances in the 50 Hz range.

Once the transfer function data is obtained, the MATLAB System Identification Toolbox functions are used in a script to generate the necessary poles and zeros to put into the SIMULINK environment. An optimization is used to minimize a cost function that is the difference of the measured output and the predicted output of the model. Here the measured output is the data obtained using Welch's method. A detailed description of the system identification process can be found in Sugiyama (Ref. 24). The end result is a continuous time state space model with various sizes of state vectors fitting the standard form in Equation (29):

$$\dot{x}(t) = Ax(t) + Bu(t)$$
$$y(t) = Cx(t) + Du(t) \tag{29}$$

Bode plots of the state space transfer functions are then compared with the bode plot of the estimated transfer function to ensure an acceptable match of the data. This can be illustrated in Figure 15 for inlet exit pressure to low-pressure spool rotational speed, starting with a second order approximation and ranging to an eighth order.

An adequate approximation of the transfer function estimate is typically achieved for the dynamics found in these engines with a model between a second and eighth order. In some cases higher order system estimation is necessary. This is typically for those dynamics that are highly nonlinear, as is found to be the case for the low-pressure shaft speed to thrust approximation. Once the order is selected, the state space model is altered using common MATLAB tools to be placed in zero-pole-gain form. A plot of the fitted sixth order estimation for the inlet exit pressure disturbance to a low-pressure spool speed can be seen in Figure 16.

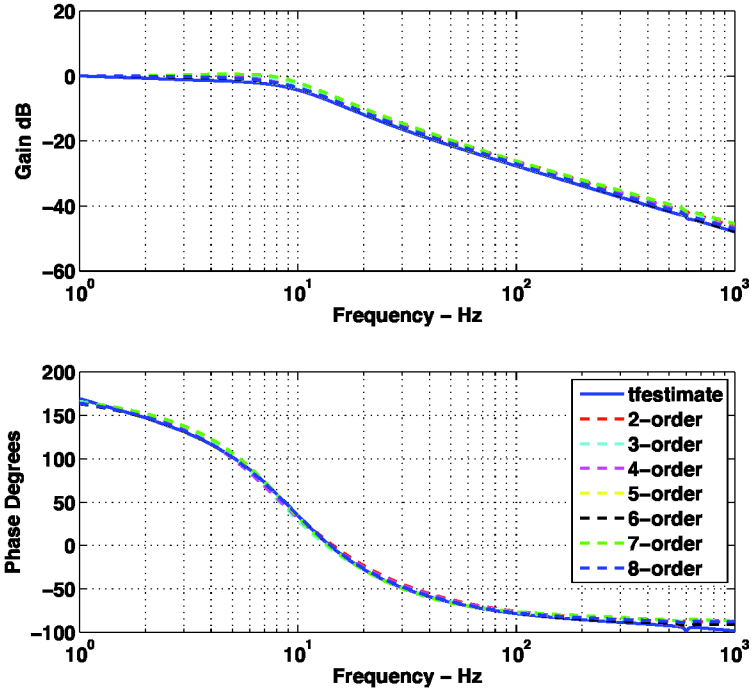

Figure 15.—Multiple order estimation for an inlet exit pressure disturbance and low-pressure spool speed response.

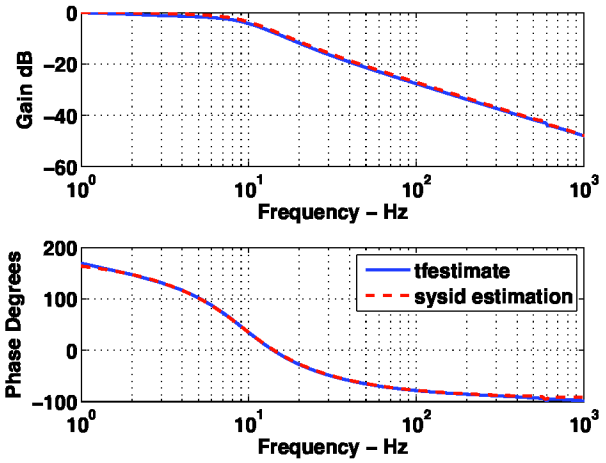

Figure 16.—Sixth order estimation of the inlet exit pressure to low-pressure spool speed.

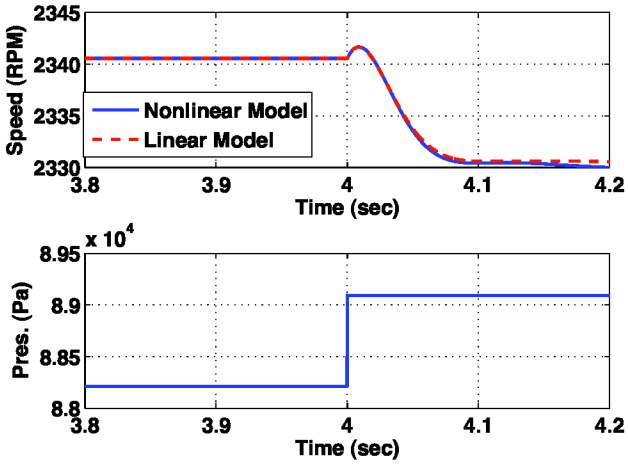

Figure 17.—Comparison of linear and nonlinear model for low-pressure shaft speed.

This approach to developing a linear model is used with a high degree of success. The input and output linear responses developed this way are very comparable to results obtained from the turbofan model about this linearization point. While the inlet exit pressure is used here to illustrate the approach, the same approach is used to obtain the linear models for the other relevant dynamics. For a final check, both the nonlinear and linear model are subjected to a step disturbance in the inlet exit pressure shown in Figure 17. The linear model closely tracks the nonlinear dynamics, and provides confidence in the linearization.

However, an issue can arise utilizing this approach while developing a linear system. The state-space model obtained can contain values along the **B** vector, instead of having only one nonzero term. This is not inherently a problem, however when implementing a classical control design approach, this can lead to problems. In altering the state-space model to a zero-pole-gain formation, a non-single value **B** vector creates an offset in the phase. The offset is not an issue when it is a constant offset and one is only concerned about the output values from the estimated transfer function. However, it does become a problem in control design, because the bandwidth of the system is significantly altered.

To still utilize the control design approach and take advantage of the quick automated estimation routine, a transfer function that will be directly used for control purposes cannot have the phase offset. The phase offset is the result of there being right half plane zeros—meaning the roots pertaining to the polynomial of the transfer function's numerator have positive values. Remembering from basic controls that the roots of the denominator are those that deal with the stability, and thus the system is still stable with right half plane zeros (Ref. 25). The real problem occurs when shaping the controller, because the dynamics are incorrect. For the few cases where this can emerge, the zero-pole-gain transfer function is used as a starting point. However, the actual fitting of the Bode plot is done by hand to eliminate the phase offset.

Future Work

Future work in this area will include the development of the control algorithm for the turbofan engine and a nonlinear inlet model with respective controls development. Once the linear plants are obtained the control design can take place. The approach to be used in future work comes from the loop shaping methodologies laid out by Kopasakis that account for design specifications (Ref. 26). Loop shaping is a linear controls design methodology that requires the nonlinear engine model to be represented as a family of linearized plants. This method is utilized for its ability to provide a more structured approach while taking into account the transient response, stability, disturbance attenuation, and most importantly the capabilities and limitations of the plant and its associated actuation system. Linear models can serve as a controls development environment, but final verification should be done using the nonlinear models. Improved fidelity of the engine model to investigate surge and rotating stall could be added to allow for a further understanding of the impacts of events that could result in an inlet unstart. Verification and validation of the turbofan model still needs to be conducted for the dynamic responses. Once the individual models are complete the overall propulsion system model comprising the inlet and engine should be developed. Finally, as the propulsion system tools are matured, the integration with the airframe dynamics model developed by NASA Langley is required along with the development of the flow field interface interconnecting the two models.

Once the control design is finished one block of the overall propulsion system model can be considered complete. Currently work is being done to develop the inlet model and controls, which will be integrated together in future work. To obtain a sense of how this work fits into the larger APSE task at NASA Glenn Figure 18 provides a schematic of the models being developed.

To start the simulation, free stream static conditions of pressure, temperature, and Mach number are applied to the inlet model. The inlet model then calculates the exit total pressure and temperature, all while controlling the normal shock position. This establishes one of the two interfaces that are required for the model, due to the nature of subsonic fluid dynamics after the normal shock at the inlet throat. Airflow properties at the inlet exit are used as the engine LPC inlet conditions. The engine then uses the

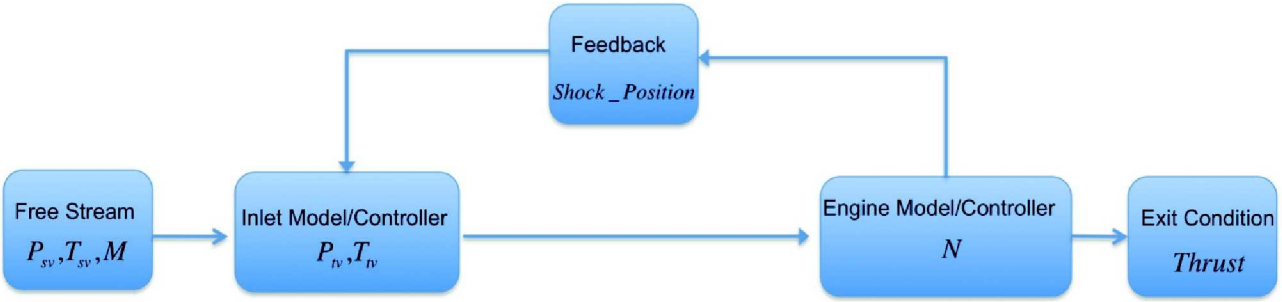

Figure 18.—Overall APSE Propulsion System Schematic.

compressor inlet conditions to obtain exit flow properties that can be used to calculate the thrust, all while controlling the engine rotational speed. For a given operating condition, the speed of the engine can be related to the mass flow at the compressor inlet through transfer functions. The mass flow at the compressor inlet can act as an inlet exit plane disturbance, which will have an impact on the normal shock position due to the flow being subsonic and traversing upstream. A transfer function is used to establish the relationship between the downstream mass flow and the normal shock position, allowing for the required feedback of a flow property in subsonic flow. The flow properties at the engine exit can be used to calculate the engine thrust or the engine speed can be directly related to the thrust produced by the propulsion system using transfer functions.

Conclusion

A modeling strategy for a nonlinear turbofan engine is outlined using a lump volume approach. Each of the major components is modeled as its own separate volume using performance maps and the conservation equations of continuity, momentum, and energy. It was found in the modeling development that starting with individual components and then building up to the whole model allowed for easier trouble shooting throughout the process. The turbofan simulation closely approximates an engine suitable for a supersonic business jet, and was shown to have good steady state matching at the cruise condition. Preliminary investigations of the transient simulations revealed expected trends, however more verification and validation is required. Using the nonlinear output data from the simulation, a linearization method was also established to support later controls development using the loop shaping methodology. A comparison was done using representative transfer function dynamics to the nonlinear model, thus providing confidence in the linearization approach. The work presented provides a reasonable approach to the propulsion-modeling element for the APSE task and allows for easy adaptation as the project matures.

Appendix

High Pressure Compressor

$$\frac{d}{dt}\rho_{hpc,sv} = \frac{1}{V_{hpc}}\left(\dot{W}_{hpc} - \dot{W}_{cb} - W_{\text{bleed}}\right) \tag{30}$$

$$\frac{d}{dt}\dot{W}_{hpc} = \frac{A_{hpc}}{l_{hpc}}\left(P_{hpc,tc} - P_{hpc,tv}\right)\left\{1 + \frac{\gamma_{hpc}-1}{2}M^2\right\}^{\frac{-\gamma_{hpc}}{\gamma_{hpc}-1}} \tag{31}$$

$$\frac{d}{dt}\left(T_{hpc,sv}\rho_{hpc,sv}\right) = \frac{\gamma_{hpc}}{V_{hpc}}\left(T_{hpc,tc}\dot{W}_{hpc} - T_{hpc,tv}\dot{W}_{cb} - T_{hpc,tv}\dot{W}_{\text{bleed}}\right) \tag{32}$$

Combustor

$$\frac{d}{dt}\rho_{cb,sv} = \frac{1}{V_{cb}}\left(\dot{W}_{cb} - \dot{W}_{\dot{f}} - W_{hpt}\right) \tag{33}$$

$$\frac{d}{dt}\dot{W}_{cb} = \frac{A_{cb}}{l_{cb}}\left(\left(P_{hpc,tv} - P_{cb,tv}\right) - \Delta P_{cb,tv}\right) \tag{34}$$

$$\frac{d}{dt}\left(T_{cb,sv}\rho_{cb,sv}\right) = \frac{\gamma_{cb}}{V_{cb}}\left(T_{hpc,tv}\dot{W}_{cb} + T_{cb,tv}\dot{W}_{\dot{f}} - T_{cb,tv}\dot{W}_{hpt} + \frac{\eta_{cb}}{c_p}\dot{W}_{\dot{f}}h_c\right) \tag{35}$$

High Pressure Turbine

$$\frac{d}{dt}\rho_{hpt,sv} = \frac{1}{V_{hpt}}\left(\dot{W}_{hpt} - \dot{W}_{hpt,\text{cool}} - W_{lpt}\right) \tag{36}$$

$$\frac{d}{dt}\dot{W}_{hpt} = \frac{A_{hpt}}{l_{hpt}}\left(P_{hpt,tc} - P_{hpt,tv}\right)\left\{1 + \frac{\gamma_{hpt}-1}{2}M^2\right\}^{\frac{-\gamma_{hpt}}{\gamma_{hpt}-1}} \tag{37}$$

$$\frac{d}{dt}\left(T_{hpt,sv}\rho_{hpt,sv}\right) = \frac{\gamma_{hpt}}{V_{hpt}}\left(T_{hpt,tc}\dot{W}_{hpt} + T_{hpc,tv}\dot{W}_{hpt,\text{cool}} - T_{hpt,tv}\dot{W}_{lpt}\right) \tag{38}$$

Low Pressure Turbine

$$\frac{d}{dt}\rho_{lpt,sv} = \frac{1}{V_{lpt}}\left(\dot{W}_{lpt} - \dot{W}_{lpt,\text{cool}} - W_{ab}\right) \tag{39}$$

$$\frac{d}{dt}\dot{W}_{lpt} = \frac{A_{lpt}}{l_{lpt}}\left(P_{lpt,tc} - P_{lpt,tv}\right)\left\{1 + \frac{\gamma_{lpt}-1}{2}M^2\right\}^{\frac{-\gamma_{lpt}}{\gamma_{lpt}-1}} \tag{40}$$

$$\frac{d}{dt}\left(T_{lpt,sv}\rho_{lpt,sv}\right)=\frac{\gamma_{lpt}}{V_{lpt}}\left(T_{lpt,tc}\dot{W}_{lpt}-T_{hpc,tv}\dot{W}_{lpt,\text{cool}}-T_{lpt,tv}\dot{W}_{ab}\right) \tag{41}$$

Mixer—Afterburner

$$\frac{d}{dt}\rho_{ab,sv}=\frac{1}{V_{ab}}\left(\dot{W}_{ab}+\dot{W}_{ab,\text{fuel}}+\dot{W}_{\text{bypass}}-\dot{W}_{z}\right) \tag{42}$$

$$\frac{d}{dt}\dot{W}_{ab}=\frac{A_{ab}}{l_{ab}}\left(\left(P_{lpt,tv}-P_{ab,tv}\right)-\Delta P_{ab}\right)\left\{1+\frac{\gamma_{ab}-1}{2}M^{2}\right\}^{\frac{-\gamma_{ab}}{\gamma_{ab}-1}} \tag{43}$$

$$\frac{d}{dt}\left(T_{ab,sv}\rho_{ab,sv}\right)=\frac{\gamma_{ab}}{V_{ab}}\left(T_{ab,tc}\dot{W}_{ab}+Q_{ab}+T_{lpc,tv}\dot{W}_{\text{bypass}}-T_{ab,tv}\dot{W}_{z}\right) \tag{44}$$

References

1. Cohen, P., Long-Davis, M. and Povinelli, L. Fundamental Aeronautics Program - Supersonics Project. NASA Reference Document, 2006.
2. Candel, S. Concorde and the Future of Supersonic Transport. Journal of Propulsion and Power, 2004, Vol. 20, No. 1.
3. Chudoba, B., Colman, G., Roberts, K., Mixon, B., Mixon, B., Oza, A. and Czysz, P.A. What Price Supersonic Speed? - A Design Anatomy of Supersonic Transportation - Part 1. In AIAA, ed. 45th AIAA Aerospace Sciences Meeting and Exhibit Reno, NV, 2007.
4. Kopasakis, G., Connolly, J., Paxson, D. and Ma, P. Volume Dynamics Propulsion System Modeling for Supersonics Vehicle Research. NASA Technical Memorandum, 2008 (NASA/TM—2008-215172).
5. Pratt & Whitney , W.P.B. and General Electric Aircraft Engines, C. Critical Propulsion Components: Summary, Introduction, and Propulsion Systems Studies. NASA Contractor Report, 2005, VOL 1. (NASA/CR—2005-213584)
6. Daniele, C.J., Krosel, S.M., Szuch, J.R. and Westerkamp, E.J. Digital Computer Program for Generating Dynamic Turbofan Engine Models (DIGTEM). NASA Technical Memorandum, 1983 (TM–83446).
7. Schobeiri, M.T., Attia, M. and Lippke. Nonlinear Dynamic Simulation of Single- and Multispool Core Engines, Part I: Computational Method. Journal of Propulsion and Power, 1994, Vol. 10, No. 6.
8. Szuch, J.R. HYDES - A Generalized Hybrid Computer Program for Studying Turbojet or Turbofan Engine Dynamics. NASA Technical Memorandum, 1974 (NASA TM X–3014).
9. Stults, I., Wilson, J.S., Beisecker, E., Morris, S., Leahu-Aluas, I. and Marvis, D. The Conceptual Design of CELESTE: a Cost-Effective, Low-Noise, Efficient, SBJ Turbofan Engine. 41st AIAA/ASME/SAE/ASEE Joint Propulsion Conference & Exhibit (AIAA, Tucson, AZ, 2005).
10. Parker, K.I. and Guo, T.H. Development of a Turbofan Engine Simulation in Graphical Simulation Environment. NASA Technical Memorandum, 2003 (NASA/TM—2003-212543).
11. Fredrick, D.K. and DeCastro, J.A. User's Guide for the Commercial Modular Aero-Propulsion System Simulation (C-MAPPS). NASA Technical Memorandum, 2007 (NASA/TM—2007-215026).
12. Seldner, K., Mihaloew, J.R. and Blaha, R.J. Generalized Simulation Technique for Turbojet Engine System Analysis. NASA Technical Note, 1972 (TN-D-6610).
13. Lytle, J. The Numerical Propulsion System Simulation: A Multidisciplinary Design System for Aerospace Vehicles. NASA Technical Memorandum, 1999 (NASA/TM—1999-209194).

14. Stueber, T.J. and Melcher, K.J. J85-13 Turbojet Engine Model for Propulsion System Control Studies. NASA Technical Paper, 2004 (NASA/TP—2004-212223).
15. Kopasakis, G. High Frequency Adaptive Instability Suppression Controls in a Liquid-Fueled Combustor. In AIAA, ed. AIAA JPC, Huntsville, AL, 2003).
16. Ames Research Center, N. Equations, Tables, and Charts for Compressible Flow. NACA Research Memorandum, 1953, 69.
17. Hill, P. and Peterson, C. Mechanics and Thermodynamics of Propulsion. Addison Wesley Publications, Reading, MA, 1992.
18. Bogacki, P. and Shampine, L.F. A 3(2) pair of Runge-Kutta formulas. Applied Math Letters, 1989, Vol. 2, pp. 1-9.
19. Khalid, S.J. and Hearne, R.E. Enhancing Dynamic Model Fidelity for Improved Prediction of Turbofan Engine Transient Performance. AIAA/SAE/ASME 16th Joint Propulsion Conference, Hartford, CT, 1980.
20. Schobeiri, M.T., Attia, M. and Lippke. Nonlinear Dynamic Simulation of Single- and Multispool Core Engines, Part II: Simulation, Code Validation. Journal of Propulsion and Power, 1994, Vol. 10 (No. 6).
21. Chun, K.S. and Swanson, D.B. Dynamic Simulation of Supersonic Inlet and Engine. AIAA Transport Aircraft Design & Operations Meeting, Seattle, WA, 1964.
22. Welch, P.D. The Use of Fast Fourier Transform for the Estimation of Power Spectra: A Method Based on Time Averaging Over Short, Modified Periodograms. IEEE Transactions Audio Electroacoustics, 1967, VOL. AU-15, 70-73.
23. Perry, B., Silva, W., Florance, J., Wieseman, C., Pototzky, A., Sanetrik, M., Scott, R., Keller, D. and Cole, S. Plans and Status of Wind-Tunnel Testing Employing an Aeroservoelastic Semispan Model. In AIAA, ed. 48th AIAA/ASME/ASCE/AHS/ASC Structures, Structural Dynamics, and Materials Conference (AIAA, Honolulu, HI, 2007).
24. Sugiyama, N. Derivation of System Matrices from Nonlinear Dynamic Simulation of Jet Engines. Journal of Guidance, Control, and Dynamics, 1994, Vol. 17, No. 6.
25. Mutambara, A. Design and Analysis of Control Systems. (CRC Press, New York, 1999).
26. Kopasakis, G. Feedback Control Systems Loop Shaping Design with Practical Considerations. NASA Technical Memorandum, 2007 (NASA/TM—2007-215007).

REPORT DOCUMENTATION PAGE		Form Approved OMB No. 0704-0188

1. REPORT DATE *(DD-MM-YYYY)*	2. REPORT TYPE	3. DATES COVERED *(From - To)*
01-05-2010	Technical Memorandum	

4. TITLE AND SUBTITLE
Turbofan Volume Dynamics Model for Investigations of Aero-Propulso-Servo-Elastic Effects in a Supersonic Commercial Transport

5a. CONTRACT NUMBER

5b. GRANT NUMBER

5c. PROGRAM ELEMENT NUMBER

6. AUTHOR(S)
Connolly, Joseph, W.; Kopasakis, George; Lemon, Kimberly, A.

5d. PROJECT NUMBER

5e. TASK NUMBER

5f. WORK UNIT NUMBER
WBS 984754.02.07.03.20.02

7. PERFORMING ORGANIZATION NAME(S) AND ADDRESS(ES)
National Aeronautics and Space Administration
John H. Glenn Research Center at Lewis Field
Cleveland, Ohio 44135-3191

8. PERFORMING ORGANIZATION REPORT NUMBER
E-17107

9. SPONSORING/MONITORING AGENCY NAME(S) AND ADDRESS(ES)
National Aeronautics and Space Administration
Washington, DC 20546-0001

10. SPONSORING/MONITOR'S ACRONYM(S)
NASA

11. SPONSORING/MONITORING REPORT NUMBER
NASA/TM-2010-216069

12. DISTRIBUTION/AVAILABILITY STATEMENT
Unclassified-Unlimited
Subject Category: 07
Available electronically at http://gltrs.grc.nasa.gov
This publication is available from the NASA Center for AeroSpace Information, 443-757-5802

13. SUPPLEMENTARY NOTES

14. ABSTRACT
A turbofan simulation has been developed for use in aero-propulso-servo-elastic coupling studies, on supersonic vehicles. A one-dimensional lumped volume approach is used whereby each component (fan, high-pressure compressor, combustor, etc.) is represented as a single volume using characteristic performance maps and conservation equations for continuity, momentum and energy. The simulation is developed in the MATLAB/SIMULINK (The MathWorks, Inc.) environment in order to facilitate controls development, and ease of integration with a future aero-servo-elastic vehicle model being developed at NASA Langley. The complete simulation demonstrated steady state results that closely match a proposed engine suitable for a supersonic business jet at the cruise condition. Preliminary investigation of the transient simulation revealed expected trends for fuel flow disturbances as well as upstream pressure disturbances. A framework for system identification enables development of linear models for controller design. Utilizing this framework, a transfer function modeling an upstream pressure disturbance's impacts on the engine speed is developed as an illustrative case of the system identification. This work will eventually enable an overall vehicle aero-propulso-servo-elastic model.

15. SUBJECT TERMS
Turbofan engines

16. SECURITY CLASSIFICATION OF:			17. LIMITATION OF ABSTRACT	18. NUMBER OF PAGES	19a. NAME OF RESPONSIBLE PERSON
a. REPORT	b. ABSTRACT	c. THIS PAGE			STI Help Desk (email:help@sti.nasa.gov)
U	U	U	UU	29	19b. TELEPHONE NUMBER *(include area code)* 443-757-5802